Biophysical Journal
Article

Biophysical Society

Sustained α-catenin Activation at E-cadherin Junctions in the Absence of Mechanical Force

Kabir H. Biswas,[1,*] Kevin L. Hartman,[1,2] Ronen Zaidel-Bar,[1,3,*] and Jay T. Groves[1,2,3,*]
[1]Mechanobiology Institute, National University of Singapore, Singapore, Singapore; [2]Department of Chemistry, University of California, Berkeley, Berkeley, California; and [3]Department of Biomedical Engineering, National University of Singapore, Singapore, Singapore

ABSTRACT Mechanotransduction at E-cadherin junctions has been postulated to be mediated in part by a force-dependent conformational activation of α-catenin. Activation of α-catenin allows it to interact with vinculin in addition to F-actin, resulting in a strengthening of junctions. Here, using E-cadherin adhesions reconstituted on synthetic, nanopatterned membranes, we show that activation of α-catenin is dependent on E-cadherin clustering, and is sustained in the absence of mechanical force or association with F-actin or vinculin. Adhesions were formed by filopodia-mediated nucleation and micron-scale assembly of E-cadherin clusters, which could be distinguished as either peripheral or central assemblies depending on their relative location at the cell-bilayer adhesion. Whereas F-actin, vinculin, and phosphorylated myosin light chain associated only with the peripheral assemblies, activated α-catenin was present in both peripheral and central assemblies, and persisted in the central assemblies in the absence of actomyosin tension. Impeding filopodia-mediated nucleation and micron-scale assembly of E-cadherin adhesion complexes by confining the movement of bilayer-bound E-cadherin on nanopatterned substrates reduced the levels of activated α-catenin. Taken together, these results indicate that although the initial activation of α-catenin requires micron-scale clustering that may allow the development of mechanical forces, sustained force is not required for maintaining α-catenin in the active state.

INTRODUCTION

Epithelial tissue integrity is maintained by the formation of adherens junctions between adjacent cells. These junctions are constituted by a calcium-dependent homophilic interaction between the transmembrane adhesion protein E-cadherin between apposing cells. A loss of E-cadherin function due to mutations in the protein results in a loss of cohesion between cells, which leads to epithelial tissue deformation and may contribute to cancer metastasis (1). E-cadherin is a multidomain protein consisting of five extracellular cadherin domains (ECD), a transmembrane domain, and a catenin-binding intracellular domain (ICD) (2–4). While the interaction between the E-cadherin ECDs from apposed cells physically holds the cells together, the E-cadherin-ICD interacts with the actin cytoskeleton by forming a tertiary complex with β-catenin and α-catenin (5–8). The integration of E-cadherin ECD (E-cad-ECD) and E-cad-ICD-mediated interactions allows the mechanical coupling of adhering cells in the epithelial tissue and provides the potential for intercellular communication (9,10).

Epithelial cells sense mechanical signals from the cellular microenvironment and remodel their adhesions as a consequence. Strengthening of adhesion has been postulated to be mediated by α-catenin, which undergoes a force-dependent activation from a closed to an open conformation, allowing increased binding to the F-actin cytoskeleton as well as to vinculin (11–15). Force-dependent conformational changes in α-catenin have been independently observed in a multitude of experiments. These include in vitro single-molecule force spectroscopy experiments using purified proteins (12,14), and binding of a conformation-specific antibody (α18) in cells (11) and in live cells using an intramolecular Förster resonance energy transfer (FRET)-based assay (13). Although the crystal structure of homodimeric α-catenin revealed structural details of the closed conformation (16), the structure of the open conformation is not known so far. In addition to α-catenin, vinculin, which is well known for its critical role in mechanical signal transduction at focal adhesions, is enriched at adherens junctions upon an increase in cellular actomyosin tension (17,18). Vinculin is structurally homologous to α-catenin and undergoes a similar closed-to-open conformational activation that allows it to interact

Submitted April 4, 2016, and accepted for publication June 24, 2016.
*Correspondence: mbikhb@nus.edu.sg or zaidelbar@gmail.com or jtgroves@lbl.gov
Editor: Michael Dustin.
http://dx.doi.org/10.1016/j.bpj.2016.06.027

with α-catenin via its head domain (15,19,20). However, in the absence of force, its tail domain outcompetes α-catenin for binding to its head domain (15,21).

Here, we used a nanopatterned supported lipid bilayer platform (22,23) to study the role of micron-scale assembly of E-cadherin clusters in mechanotransduction at adherens junctions. Supported lipid bilayers are suited for such studies because they allow membrane-associated proteins to be organized into micron-scale assemblies, a process that can be physically perturbed by the application of nanopatterned substrates to elucidate the role of assembly in signal transduction (24–28). Mobility-dependent assembly, and physical perturbation of such assemblies could not be achieved together in other cell adhesion assays such as monolayer cell cultures or those that involve display of protein on solid surfaces. Cellular extension and retraction of filopodia on E-cad-ECD-functionalized bilayers nucleates specific adhesion and clustering of cell-surface E-cadherin with bilayer-bound E-cad-ECD (22). These clusters then accumulate with previously formed clusters, resulting in the assembly of extended E-cadherin-mediated adhesions at the cell-bilayer interface.

These adhesion assemblies contain E-cadherin in complex with key adaptor proteins, including β- and α-catenin, and can be distinguished as peripheral or central assemblies based on their spatial localization. Although the peripheral assemblies associate with F-actin, vinculin, and phosphorylated myosin light chain, the central assemblies do not. Both types of E-cadherin assemblies, however, contain α-catenin in the active, open conformation, as determined by binding of the isolated vinculin-head domain or the conformation-specific α18 antibody. Furthermore, the release of cellular applied tension by pharmacological inhibition of actomyosin contractility also fails to switch α-catenin to the inactive, closed state. The use of nanopatterned supported bilayers, in which grids of metallic structures fabricated onto the underlying substrate create barriers to the lateral mobility of supported-bilayer components, leads to a systematic reduction in the amount of active α-catenin. On these patterned substrates, E-cad-ECD in the supported bilayer is free to assemble locally into small-scale clusters, but micron-scale movements, including the filopodia-mediated nucleation process, are blocked (22,25,29,30). This suggests that α-catenin becomes activated during the nucleation process that initially activates E-cadherin assembly and adhesion. Once activated, however, α-catenin does not revert to the inactive state, even in the absence of mechanical force. The consequences of this observation on our understanding of the mechanism by which cadherin-mediated adherens junctions sense force will be discussed.

MATERIALS AND METHODS

Details regarding the materials and methods used in this work are available in Supporting Materials and Methods in the Supporting Material. Briefly, vesicles prepared using 1,2-dioleoyl-*sn*-glycero-3-phosphocholine (DOPC) and 1,2-dioleoyl-*sn*-glycero-3-[(N-(5-amino-1-carboxypentyl)iminodiacetic acid)succinyl] nickel salt (Ni-NTA-DOGS) were used to prepare bilayers by the vesicle fusion method (31). E-cad-ECD containing a C-terminal His_6 was attached to bilayers via Ni-NTA-poly-His interaction (32). FRAP was performed by illuminating a small field of view (15–30 μm diameter) at high intensity, followed by continued imaging to observe recovery of fluorescence. Hybrid E-cadherin adhesions were reconstituted by seeding MKN28-E-cad-GFP cells (22), and adhesion was observed using a 100× objective in an Eclipse Ti inverted microscope in either total internal reflection fluorescence (TIRF) or confocal mode. Images were collected in Metamorph (Molecular Devices, Sunnyvale, CA) and analyzed with either ImageJ (NIH, Bethesda, MD) or Fiji (33). For ratiometric analysis, images were registered using the TurboReg plugin (34). Micron-scale patterned substrates were prepared by deep UV-etching PLL-PEG coating (35), and nanoscale chromium-patterned substrates were prepared by nano-imprinting (24). Cells were stained with phalloidin to visualize F-actin or with protein-specific antibodies to visualize their localization. Activated α-catenin was visualized either by expressing vinculin-head-mCherry (chicken; amino acid residues 1–258) (12) or by staining with the conformation-specific α18 antibody (11). Cells were treated with 50 μm of either Y-27632 or blebbistatin for 30 min to reduce actomyosin tension.

RESULTS

In vitro reconstitution of E-cadherin adhesion in a live cell/supported lipid bilayer system

Here, we studied the interaction between E-cadherin and the actin cytoskeleton in a hybrid setting wherein one of the cells was replaced with a nanopatterned supported lipid bilayer displaying E-cad-ECD (Fig. 1 *A*). We employed a previously described strategy to display purified, recombinant human E-cad-ECD (Fig. S1 *A*) on supported lipid bilayers (22,32). Epithelial MKN28 cells expressing GFP-tagged E-cadherin (MKN28-E-cad-GFP) (8,22) were used to enable visualization of junctions that formed between cells and the bilayer. Functionalizing bilayers with poly-His containing E-cad-ECD at high density resulted in a reduction in mobility, as seen in a fluorescence recovery after photobleaching (FRAP) experiment (Fig. S1, *B* and *C*), thereby creating a proper physical microenvironment for junction formation (22).

A significantly higher number of cells remained adhered to bilayers containing E-cad-ECD compared with control bilayers that did not contain E-cad-ECD (Fig. 1 *B*), indicating that the protein that was displayed on the bilayer surface was adhesive. We utilized TIRF microscopy to observe enrichment and clustering of E-cadherin-GFP at the cell-bilayer interface (36). Cells seeded on E-cad-ECD-functionalized bilayers showed an enrichment of cellular E-cadherin-GFP at the cell-bilayer interface (Fig. 1 *C*), which was not observed on bilayers lacking E-cad-ECD (but containing Ca^{2+} ions) or in the absence of Ca^{2+} ions (Fig. 1 *C*). Additionally, cells seeded on E-cad-ECD bilayers showed significantly larger contact areas compared with cells on bilayers without E-cad-ECD (Fig. S1 *D*). Mature adhesions were formed by the

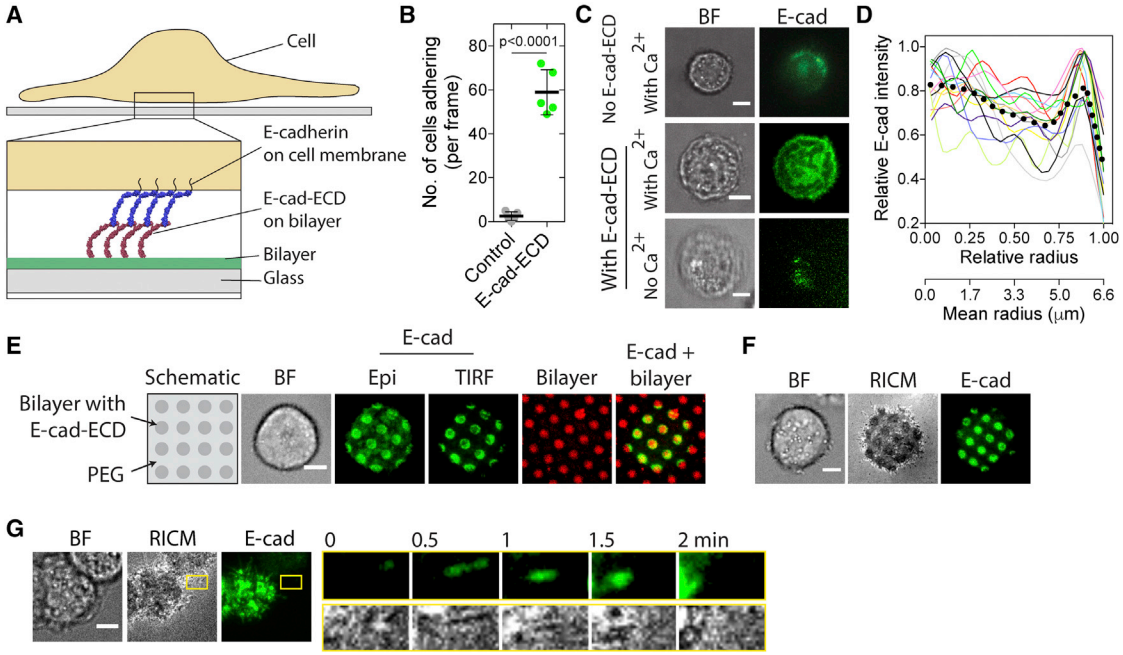

FIGURE 1 E-cadherin adhesion on a supported lipid bilayer. (*A*) Schematic representation of a cell forming an adhesion on an E-cad-ECD-functionalized bilayer. (*B*) Graph showing a comparison of the number of cells adhering to control (without E-cad-ECD) versus E-cad-ECD-functionalized bilayers. The data shown are from multiple independent experiments and the *p*-value was obtained from an unpaired *t*-test. (*C*) Bright-field (BF) and TIRF microscopy images of E-cadherin in cells seeded on control (without E-cad-ECD) or on E-cad-ECD-functionalized bilayers in the absence and presence of 2 mM $CaCl_2$, respectively. Note the extensive zone of cellular E-cadherin enrichment on E-cadherin bilayers in the presence of $CaCl_2$. (*D*) Plot showing multiple individual radial E-cadherin intensity profiles obtained from confocal images of adhesions formed by cells on E-cad-ECD-functionalized bilayers, revealing a peak at the cell periphery and random distribution of E-cadherin clusters within the adhesions. Original individual intensity profiles were smoothed with the average of three data points. The lower *x* axis panel shows the average cell contact radius, revealing micron-scale features of E-cadherin in individual radial profiles. The dotted black curve shows the average profile of all the 15 cells shown individually. (*E*) Schematic of a micropatterned substrate containing 2 μm discs of supported lipid bilayers functionalized with E-cad-ECD on a PEG surface. BF, epifluorescence (Epi), and TIRF images of an adhering cell on the micropatterned substrate. Bilayer discs are shown in red. Note that the enrichment of cellular E-cadherin coincides with regions of the substrate containing E-cad-ECD-functionalized bilayer discs. (*F*) BF, RICM, and TIRF images of an adhering cell on micropatterned substrate containing 2 μm discs of bilayers functionalized with E-cad-ECD, showing loss of RICM intensity due to interference at regions containing E-cadherin clusters. (*G*) TIRF and RICM images of a cell forming an adhesion on an E-cad-ECD bilayer, showing the addition of E-cadherin clusters formed by retracting filopodia, leading to the formation of large assemblies of E-cadherin at the adhesion. Scale bar, 5 μm.

dynamic movement of clusters at the cell-bilayer interface (Fig. S1 *E*), and the fluorescence intensity measured from the time-lapse TIRF images plateaued in ~30 min, with a mean $t_{1/2}$ for junction formation of 7.5 min (Fig. S1 *F*). The kinetics of adhesion formation observed in the hybrid format here is consistent with time frames reported for junction formation between two live cells (37). Additionally, mature adhesions showed very little recovery of E-cadherin fluorescence intensity in a FRAP experiment (Fig. S1 *G*), indicating that a large fraction of E-cadherin is immobilized upon adhesion formation, which is a characteristic feature of stable E-cadherin junctions (37).

Cells forming adhesion on the E-cadherin bilayers typically showed a ring of E-cadherin clusters at the periphery and some clusters at the central part of the cell-bilayer contact. Indeed, an analysis of E-cadherin intensity at a large number of adhesions by radial intensity profiling revealed a consistent peak at the periphery in all cells and a random distribution of micron-scale features of E-cadherin within the central part of adhesions (Fig. 1 *D*) (24). Henceforth, we refer to these spatially segregated assemblies as peripheral and central assemblies, respectively. Further, cells seeded on micropatterned supported membrane substrates consisting of small discs of E-cad-ECD-functionalized bilayers (2 μm diameter) showed enrichment and clustering of cellular E-cadherin-GFP as well as cell membrane topography (imaged by reflection interference contrast microscopy (RICM)) in a spatially restricted manner commensurate with the bilayer micropattern (Figs. 1, *E* and *F*, and S1 *H*), indicating that the clusters of E-cadherin observed in the cells represent cellular E-cadherin molecules specifically interacting with E-cadherin molecules on the bilayer (38,39). As reported previously (22), cells extended filopodia on the bilayer, and clusters of E-cadherin that were formed by the retraction of filopodia were subsequently fused to previously assembled clusters, resulting in the formation of an extensive adhesive zone between the cell and bilayer (Fig. 1 *G*).

Spatially differentiated E-cadherin interactions with the cytoskeleton and cadhesome proteins

Having reconstituted E-cadherin adhesions on a synthetic substrate, we then investigated the association of E-cadherin clusters with the actin cytoskeleton. As shown in Fig. 2 *A*, only the peripheral assemblies of E-cadherin clusters were associated with the actin cytoskeleton at the cell-bilayer interface. In contrast to the peripheral assemblies, the central assemblies of E-cadherin did not localize with F-actin filaments. Instead, F-actin filaments were found interspersed between the central assemblies and they appeared to be anti-localized with E-cadherin assemblies at the central part of the adhesion (Fig. 2 *D*). Immunofluorescence staining of cells with anti-β-catenin (Fig. 2, *B* and *D*) and anti-α-catenin (Fig. 2, *C* and *D*) antibodies showed that both types of assemblies were associated with β- and α-catenin. Importantly, such spatial segregation of E-cadherin clusters and their spatially distinct localization with F-actin was not observed when the cells were pretreated with 50 μM Y-27632, suggesting that actomyosin tension is required for the assembly of mature adhesions (Fig. S2 *A*) (40).

Unlike β- and α-catenin, vinculin was found to be associated exclusively with peripheral E-cadherin assemblies (Fig. 3 *A*) (17,41,42). Although vinculin is thought to be recruited to E-cadherin junctions via α-catenin in a force-dependent manner, some immunoprecipitation-based reports have suggested a direct interaction of vinculin with β-catenin in MDA-MB-468 cells (18,43). To understand the mechanism of vinculin recruitment at these hybrid adhesions, we performed a pull-down experiment with purified ICD of E-cadherin and lysates prepared from MKN28-E-cadherin-GFP cells. Although both β- and α-catenin interacted with the ICD of E-cadherin, vinculin could not be detected interacting with the complex (Fig. S2 *B*). This is in agreement with results obtained from immunoprecipitation experiments with A431 and MCF-7 epithelial carcinoma cells (18), and ruled out a force-independent, direct interaction of vinculin with β-catenin in the MKN28 cells. Additionally, the inability of α-catenin to bind vinculin in this solution-based assay, where physical forces cannot be developed, suggests that the interaction between the two proteins is force dependent and requires both of them to be present in the active conformation (11,14,21).

We then investigated the localization of other cadhesome proteins that could potentially play a role in mechanotransduction at the hybrid cell-bilayer junctions. Similar to vinculin, phosphorylated myosin light chain (Fig. 3, *B* and *M*) (40,44), lipoma-preferred partner (LPP) (Fig. S3 *A*) (7), and Zyxin (Fig. S3 *B*) (45,46) localized specifically to the peripheral E-cadherin assemblies. On the other hand, IQGAP1 (47) colocalized with both peripheral and central E-cadherin clusters in a pattern similar to that of α-catenin (Fig. S3 *C*). Thus, recruitment of cadhesome proteins (8) to E-cadherin assemblies is dependent on their association with the actin cytoskeleton, consistent with differential functional roles of E-cadherin clusters at apical versus lateral junctions between epithelial cells (48).

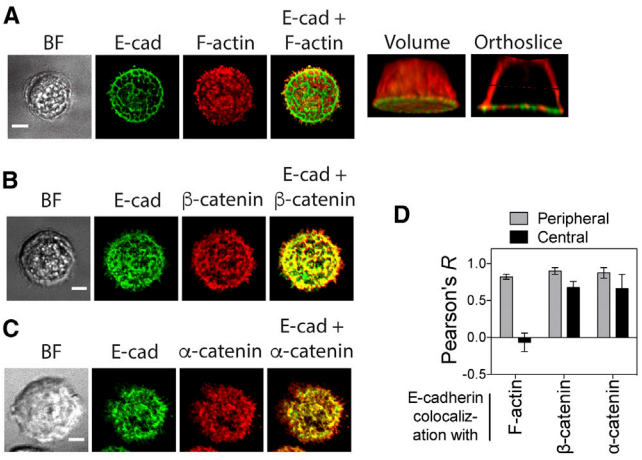

FIGURE 2 Interaction between E-cadherin assemblies and the actin cytoskeleton. (*A*) BF and confocal images of E-cadherin and F-actin (phalloidin) in cells adhering to E-cad-ECD bilayers. A volume and orthoslice reconstruction of the actin cytoskeleton and E-cadherin assemblies, performed using z-scan confocal imaging of the cell, shows a remodeled actin cytoskeleton. Note that the peripheral E-cadherin assemblies associate with F-actin, but the central assemblies do not (although intermittent patches of F-actin are present in the central part of the cell). (*B* and *C*) BF and confocal images of E-cadherin and either β-catenin (*B*) or α-catenin (*C*) in cells adhering to E-cad-ECD bilayers, showing colocalization of E-cadherin with β-catenin (*B*) or α-catenin (*C*), respectively. (*D*) Graph showing Pearson's *R*-value of E-cadherin colocalization with F-actin, β-catenin, and α-catenin in the peripheral and central clusters. Scale bar, 5 μm.

Sustained α-catenin activation in the absence of force

Force-dependent conformational activation of α-catenin has been postulated to be a key mechanotransducing signal at E-cadherin adhesions (11,12,14). We investigated the conformation of α-catenin at the cell-bilayer interface by expressing the vinculin head domain construct without the autoinhibitory tail domain (vinculin head; residues 1–258) (12) and by staining with the α18 antibody (11). Both the vinculin head and α18 bind specifically to activated α-catenin, which is thought to be the conformation that can bind F-actin and vinculin (11,12,14). These experiments revealed that α-catenin associated with both the peripheral and central assemblies of E-cadherin clusters binds the vinculin head and α18 antibody (Fig. 3, *C* and *D*), indicating that α-catenin is present in an open conformation in both types of assemblies. This result is not surprising for peripheral assemblies of E-cadherin, which colocalize with F-actin, vinculin, and phosphorylated myosin light chain (Figs. 2 *A* and 3, *A* and *B*). E-cadherin in central assemblies, on the other hand, exhibits no apparent association with the actin cytoskeleton or phosphorylated myosin light chain, and thus does not appear to be under tensile force. Although

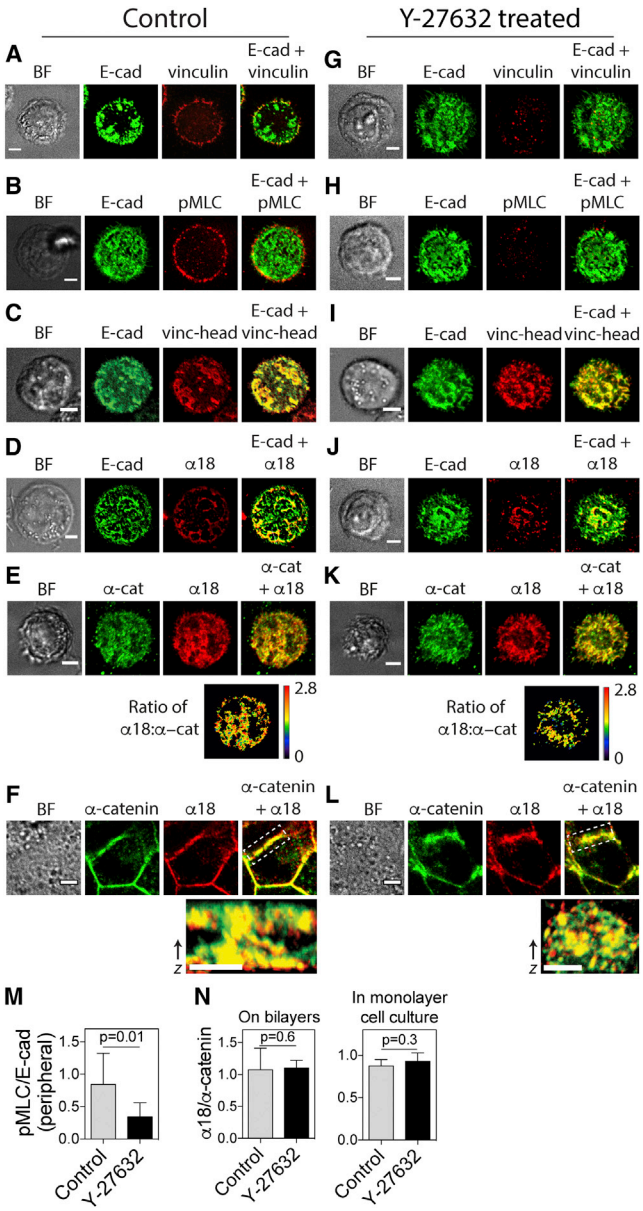

FIGURE 3 α-catenin is sustained in the active conformation irrespective of actomyosin tension. (*A–D*) BF and confocal images of cells forming junctions on E-cad-ECD-functionalized bilayers stained for stained for vinculin (*A*) or phosphorylated myosin light chain (*B*), and cells expressing the vinculin-head domain fused to mCherry (vinc-head) (*C*) and stained for the open conformation of α-catenin using the α18 antibody (11) (*D*). (*G–J*) BF and confocal images of 50 μM Y-27632-treated cells stained for vinculin (*G*) or phosphorylated myosin light chain (*H*), and cells expressing the vinculin-head domain fused to mCherry (vinc-head) (*I*) and stained for the open conformation of α-catenin using the α18 antibody (*J*) (11). (*E* and *K*) BF and confocal images of control (*E*) and Y-27632-treated (*K*) cells adhering to E-cad-ECD bilayers. Cells were stained for total α-catenin using an antibody that binds to the C-terminus of the protein independently of its conformation, and for the conformationally activated α-catenin using the α18 antibody. The lower-right panels in (*E*) and (*K*) are ratiometric images of α18 and total α-catenin staining for the respective cells. (*F* and *L*) BF and confocal images of cells forming junctions in monolayers and stained for total α-catenin and the conformationally activated α-catenin visualized with α18 antibody in control (*F*) or 50 μm Y-27632-treated (*L*) cells. (*M*) Graph showing the ratio of pMLC and E-cadherin-GFP intensities at the cell periphery in control and Y-27632-treated cells, revealing a reduction in the actomyosin tension upon Y-27632 treatment of the cells. (*N*) Graph showing the ratio of α18 and total α-catenin staining intensities in control and Y-27632-treated cells on bilayers or monolayer cultures. No significant differences are observed in the levels of activated α-catenin in control and Y-27632-treated cells. Scale bar, 5 μm.

constitutively active vinculin constructs have been shown to stabilize focal adhesion complexes (49), staining with the α18 antibody after chemical cross-linking-based fixation of the cellular proteins suggests that these results are not experimental artifacts. Further, the absence of vinculin from central E-cadherin assemblies that contain activated α-catenin indicates a more stringent autoinhibition in vinculin caused by its tail domain in the absence of an interaction with F-actin, consistent with the absence of vinculin in the pull-down experiment with the purified ICD of E-cadherin (Fig. S2 *B*) (15,19,21).

The presence of α-catenin in the active conformation in central E-cadherin assemblies, which did not associate with F-actin, was intriguing, especially considering the reversible conformational change in α-catenin observed with the use of a FRET-based sensor (13). To rule out any role of cellular actomyosin contractility in this phenomenon, we observed the effect of a reduction in actomyosin tension by treating adhering cells with pharmacological inhibitors. Treatment of cells with the ROCK inhibitor Y-27632 for 30 min after the formation of stable adhesions (60 min after seeding of cells) resulted in a decrease in the peripheral E-cadherin assemblies and a loss of vinculin and phosphorylated myosin light chain staining (Fig. 3, *G*, *H*, and *M*), thus confirming the effectiveness of the drug in reducing actomyosin contractility in the cells. However, central E-cadherin assemblies were found to be stable under Y-27632 treatment, and α-catenin that associated with these assemblies still bound both the vinculin head (Fig. 3 *I*) and the α18 antibody (Fig. 3 *J*). To obtain a more quantitative comparison of α-catenin activation, we simultaneously stained both control and Y-27632-treated cells with α18 and another antibody that binds α-catenin in a conformation-independent manner and thus reports the levels of total α-catenin (11). Whereas the α18 antibody binds to the central part of α-catenin (11), the epitope for the anti-α-catenin antibody used to stain total α-catenin lies in the C-terminus of α-catenin (residues 890–901), and therefore the two antibodies should not interfere with each other in binding to α-catenin. The relative levels of the open conformation of α-catenin were determined by a ratiometric analysis of the α18- and anti-α-catenin-stained images (11). This analysis revealed that the relative levels of conformationally active α-catenin remained unaltered upon a reduction in cellular actomyosin contractility with Y-27632 treatment (Fig. 3, *E*, *K*, and *N*). Similar results were obtained with the myosin inhibitor blebbistatin (Fig. S4 *A*). Further, these results could be recapitulated in native cell-cell junctions

formed by cells in monolayers (Figs. 3, *F*, *L*, and *N*, and S4, *B* and *C*). Thus, once α-catenin has been activated in the process of adhesion formation, it does not appear to be sensitive to cellular actomyosin contractility and remains in the active conformation in the absence of force.

Nucleation and micron-scale assembly of E-cadherin are required for the activation of α-catenin

We previously reported that E-cadherin adhesion formation involves an active nucleation process in which the retraction of filopodia over distances of a few microns results in the local enrichment of E-cadherin and stable junction formation (22). This process can be physically inhibited by the spatial mutation method, in which a patterned supported membrane is employed to control the movement and geometric assembly of cell-surface receptor proteins (23–26,28,29,50). Here, we fabricated chromium grids ranging from 500 nm to 2 μm on the glass substrate by nano-imprint lithography to physically restrict the movement of E-cadherin. Cells seeded on bilayers containing nanopatterned chromium barriers were allowed to form junctions, and a ratiometric analysis of active and total α-catenin was performed as mentioned in the previous section.

Similar nucleation and micron-scale assembly of E-cadherin clusters were observed in cells adhering to E-cadherin bilayers containing large (2 μm spacing) grids compared with cells adhering to bilayers without any barriers (off grid) (Fig. 4 *A*). This results from the fact that the filopodia retraction and micron-scale movement of E-cadherin is not significantly hindered on the large grids. However, cells that formed junctions on bilayers containing smaller grids (1 μm and 500 nm spacing), where the filopodia-driven nucleation process was impeded, showed a decrease in the micron-scale assembly of cellular E-cadherin (Fig. 4 *A*). In parallel with the reduction of micron-scale E-cadherin assemblies on small grids, we found that the ratio of α18 to total α-catenin staining intensity also decreased (20% and 46% on grid spacings of 1 μm and 500 nm, respectively, compared with the off-grid cells) (Fig. 4, *A* and *B*). Thus, filopodia retraction-mediated nucleation and micron-scale assembly of E-cadherin clusters at the cell-bilayer interface is required for the activation of α-catenin. Additionally, the changes in the relative levels of α18 binding (normalized to total α-catenin) determined in these experiments with chromium barriers of different sizes clearly establish that the α18 antibody is a reliable reporter of the α-catenin conformation.

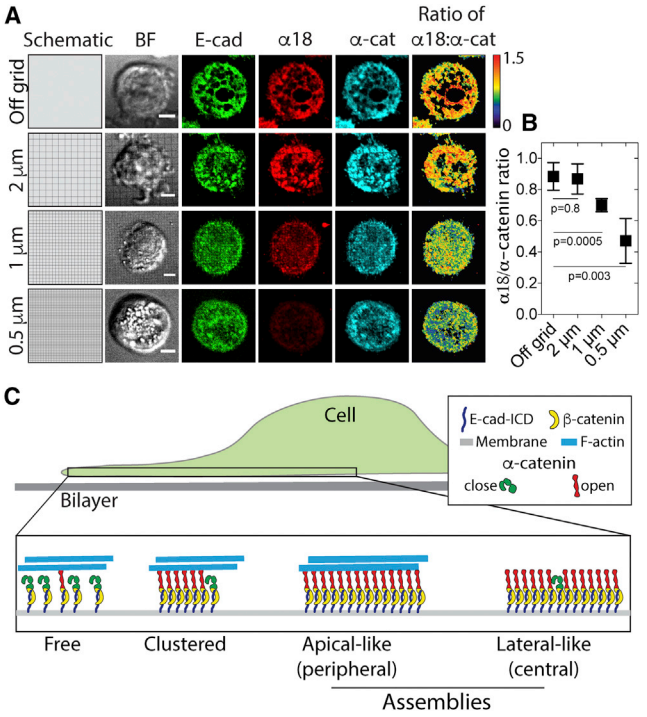

FIGURE 4 Nucleation and micron-scale assembly of E-cadherin clusters regulate the conformational activation of α-catenin. (*A*) Schematic representation of a nanopatterned supported lipid bilayer, BF and confocal images of cells adhering to the respective nanopatterned bilayers stained for total α-catenin, the open conformation of α-catenin using α18 antibody (11), and the ratio of α18 and total α-catenin intensities. Scale bar, 5 μm. (*B*) Graph showing the ratio of α18 and total α-catenin intensities (mean ± SD) obtained from multiple cells from a representative experiment. (*C*) Schematic representation of the conformational regulation of α-catenin by micron-scale assembly of E-cadherin clusters. A cell seeded on an E-cad-ECD-functionalized bilayer clusters E-cadherin by retracting filopodia. α-catenin is activated during the process of assembly of micron-scale E-cadherin clusters due to its association with the actin cytoskeleton. Once activated, α-catenin stays in that form even in the absence of its association with actin cytoskeleton as seen with the central E-cadherin assemblies, or in the absence of mechanical force as seen with the Y-27623 treatment.

DISCUSSION

Here, we report a sustained activation of α-catenin at E-cadherin adhesions in the absence of continued actomyosin tension and interaction with either F-actin or vinculin. Adhesions reconstituted on synthetic, supported lipid bilayer substrates exhibited E-cadherin in spatially and compositionally segregated peripheral and central clusters. Although a variety of junctional structures have been reported in the literature for different members of the cadherin family, studies on E-cadherin junctions formed between polarized epithelial cells, such as the MKN28 cells used here, have described two pools of E-cadherin clusters: one at the apical end of the lateral surface, termed the zonula adherens, and the other on the lateral surface below the zonula adherens (8,51,52). Based on their spatial arrangement and molecular composition, we propose that the peripheral assemblies are reflective of apical clusters that are under cellular actomyosin tension exerted through the peripherally localized actin filaments. On the other hand, the central assemblies are more analogous to lateral clusters that do not appear to be under actomyosin tension. Consistent with this, a reduction in cellular actomyosin tension resulted in a loss of the

peripheral E-cadherin assemblies concomitantly with the loss of phosphorylated myosin light chain and vinculin staining, whereas the central assemblies remained largely intact.

The persistent activation of α-catenin at E-cadherin adhesions that we describe here furthers our understanding of the mechanical regulation of cadherin adhesion. Although this is an unexpected finding, it may not be contradictory to previous studies that suggested swift changes in the levels of activated α-catenin upon an alteration in actomyosin contractility (11,13,41). Investigators have studied this activation of α-catenin both in vitro and in live cells using different tools. In vitro studies have reported either binding of the vinculin-head domain upon mechanical stretching of α-catenin (12) or a change in the α-catenin-F-actin bond lifetime under tension (14). Cell-based assays have utilized either binding of the conformation-specific α18 antibody to α-catenin (11) or a FRET-based α-catenin force sensor (13). Although they generally report a force-induced structural transition, each of these tools reports a distinct conformation or conformational transition in α-catenin (53–56). This is clear from results obtained with the FRET-based α-catenin sensor and a vinculin construct without the autoinhibitory tail (13). Although the FRET-based sensor returned almost instantaneously to the high-FRET, low-tension state upon a reduction in cellular tension, the vinculin construct stayed bound to α-catenin for a much longer period. These results suggest that the FRET-based sensor probably reports a force-dependent partial structural unfolding of α-catenin (12), and not the conformation with exposed cryptic binding sites that allow binding of interacting proteins such as vinculin. It is possible that force-induced partial unfolding of α-catenin follows exposure of the cryptic binding sites. We note that although force is a signaling *input* and is valuable to study where and when forces are applied on α-catenin, exposure of cryptic binding sites is the *response* that is critical for mechanotransduction at E-cadherin adhesions. Therefore, the activation of α-catenin that we observed here using the vinculin-head domain construct and α18 antibody is valuable for understanding α-catenin function. Also, previous cell-based studies were focused on the activation status of α-catenin only at the apical junctions. We, on the other hand, report the α-catenin activation status for both peripheral and central assemblies in parallel. This was possible primarily due to the reconstitution of adhesions on a two-dimensional bilayer surface, thus indicating the usefulness of the hybrid live cell/supported lipid bilayer system for studying cell-cell adhesion. We note that although previous studies utilized other cell lines, results presented here and previously (8,22,52) show that the MKN28 epithelial cells used here display all of the relevant features of E-cadherin adhesion and mechanotransduction. Therefore, the key observations regarding the mechanical regulation of α-catenin reported here should be relevant for other cell lines as well. The mechanism of stabilization of α-catenin in the active conformation may involve a posttranslational modification (57) or an interaction with another protein (5). The final inactivation of α-catenin may require the disengagement of E-cadherin, either by simple unbinding or by proteolytic cleavage (58), at the site of adhesion, and cellular recycling processes such as endocytosis (59).

The use of nanopatterned supported lipid bilayer substrates with physical barriers uncovered a requirement for nucleation and micron-scale assembly of E-cadherin for α-catenin activation (22). Nanopatterned substrates have been successfully employed to elucidate the role of receptor clustering in a number of cellular signaling systems, including T-cell activation, EphA2 receptor tyrosine kinase signaling, and integrin adhesion (24–26,60–66). Unlike genetic or pharmacological perturbations that may have off-target or deleterious effects (e.g., on protein stability), these nanopatterned substrates allow receptor clustering to be perturbed in a purely physical way, thereby avoiding such effects. More importantly, although mutation of the *cis*-interaction interface in E-cadherin results in a change in the dynamics of E-cadherin clusters, cells nevertheless form E-cadherin clusters (22,52,67–69), and thus the *cis*-mutant E-cadherin may not be useful for investigating the role of E-cadherin clustering. Therefore, the use of nanopatterned substrates, as described here, appears to be the only way to definitively manipulate micron-scale E-cadherin assemblies. Further, it is interesting to note that obstruction of the micron-scale clustering of E-cadherin results in a loss of α-catenin activation. This suggests that a decrease in molecular mobility, which is essential for E-cadherin adhesion formation (22), is not sufficient for development of the forces required for α-catenin activation. Instead, a local increase in the concentration of E-cadherin is required for the development of forces and activation of α-catenin. Indeed, the use of these substrates provided insights into E-cadherin adhesion and mechanotransduction that could not have been achieved in a regular cell-based assay.

In conclusion, α-catenin is activated during the initial adhesion assembly process involving filopodia retraction-mediated nucleation and clustering of E-cadherin (Fig. 4 *C*). Activated α-catenin continues to be present in the active conformation while E-cadherin clusters are dynamically organized into peripheral and lateral assemblies. Further, α-catenin does not require continuous force to maintain its open conformation. As such, α-catenin is unable to respond to changes in force in the context of an assembled E-cadherin adhesion, and is unlikely to play a role as a real-time force sensor.

SUPPORTING MATERIAL

Supporting Materials and Methods and four figures are available at http://www.biophysj.org/biophysj/supplemental/S0006-3495(16)30473-8.

AUTHOR CONTRIBUTIONS

K.H.B., R.Z.-B., and J.T.G. conceived the study. K.H.B. and K.L.H. performed experiments and analyzed data. K.H.B., K.L.H., R.Z.-B., and J.T.G. wrote the manuscript.

ACKNOWLEDGMENTS

We thank Prof. Akira Nagafuchi for the kind gift of α18 antibody, and Prof. Pakorn Kanchanawong for the vinculin-head-mCherry plasmid construct.

This work was supported by the National Research Foundation, Singapore through the Mechanobiology Institute, National University of Singapore, and Competitive Research Program grant CRP001-084 awarded to R.Z.-B. and J.T.G.

REFERENCES

1. Vasioukhin, V. 2012. Adherens junctions and cancer. *Subcell. Biochem.* 60:379–414.
2. Patel, S. D., C. P. Chen, …, L. Shapiro. 2003. Cadherin-mediated cell-cell adhesion: sticking together as a family. *Curr. Opin. Struct. Biol.* 13:690–698.
3. Brasch, J., O. J. Harrison, …, L. Shapiro. 2012. Thinking outside the cell: how cadherins drive adhesion. *Trends Cell Biol.* 22:299–310.
4. Troyanovsky, S. 2012. Adherens junction assembly. *Subcell. Biochem.* 60:89–108.
5. Zaidel-Bar, R. 2013. Cadherin adhesome at a glance. *J. Cell Sci.* 126:373–378.
6. Han, S. P., and A. S. Yap. 2012. The cytoskeleton and classical cadherin adhesions. *Subcell. Biochem.* 60:111–135.
7. Van Itallie, C. M., A. J. Tietgens, …, J. M. Anderson. 2014. Biotin ligase tagging identifies proteins proximal to E-cadherin, including lipoma preferred partner, a regulator of epithelial cell-cell and cell-substrate adhesion. *J. Cell Sci.* 127:885–895.
8. Guo, Z., L. J. Neilson, …, R. Zaidel-Bar. 2014. E-cadherin interactome complexity and robustness resolved by quantitative proteomics. *Sci. Signal.* 7:rs7.
9. Maître, J. L., H. Berthoumieux, …, C. P. Heisenberg. 2012. Adhesion functions in cell sorting by mechanically coupling the cortices of adhering cells. *Science.* 338:253–256.
10. Lecuit, T., and A. S. Yap. 2015. E-cadherin junctions as active mechanical integrators in tissue dynamics. *Nat. Cell Biol.* 17:533–539.
11. Yonemura, S., Y. Wada, …, M. Shibata. 2010. alpha-Catenin as a tension transducer that induces adherens junction development. *Nat. Cell Biol.* 12:533–542.
12. Yao, M., W. Qiu, …, J. Yan. 2014. Force-dependent conformational switch of α-catenin controls vinculin binding. *Nat. Commun.* 5:4525.
13. Kim, T. J., S. Zheng, …, Y. Wang. 2015. Dynamic visualization of α-catenin reveals rapid, reversible conformation switching between tension states. *Curr. Biol.* 25:218–224.
14. Buckley, C. D., J. Tan, …, A. R. Dunn. 2014. Cell adhesion. The minimal cadherin-catenin complex binds to actin filaments under force. *Science.* 346:1254211.
15. Ishiyama, N., N. Tanaka, …, M. Ikura. 2013. An autoinhibited structure of α-catenin and its implications for vinculin recruitment to adherens junctions. *J. Biol. Chem.* 288:15913–15925.
16. Rangarajan, E. S., and T. Izard. 2013. Dimer asymmetry defines α-catenin interactions. *Nat. Struct. Mol. Biol.* 20:188–193.
17. le Duc, Q., Q. Shi, …, J. de Rooij. 2010. Vinculin potentiates E-cadherin mechanosensing and is recruited to actin-anchored sites within adherens junctions in a myosin II-dependent manner. *J. Cell Biol.* 189:1107–1115.
18. Hazan, R. B., L. Kang, …, D. L. Rimm. 1997. Vinculin is associated with the E-cadherin adhesion complex. *J. Biol. Chem.* 272:32448–32453.
19. Izard, T., G. Evans, …, P. R. Bois. 2004. Vinculin activation by talin through helical bundle conversion. *Nature.* 427:171–175.
20. Chen, H., D. M. Choudhury, and S. W. Craig. 2006. Coincidence of actin filaments and talin is required to activate vinculin. *J. Biol. Chem.* 281:40389–40398.
21. Choi, H. J., S. Pokutta, …, W. I. Weis. 2012. αE-catenin is an autoinhibited molecule that coactivates vinculin. *Proc. Natl. Acad. Sci. USA.* 109:8576–8581.
22. Biswas, K. H., K. L. Hartman, …, J. T. Groves. 2015. E-cadherin junction formation involves an active kinetic nucleation process. *Proc. Natl. Acad. Sci. USA.* 112:10932–10937.
23. Groves, J. T., N. Ulman, and S. G. Boxer. 1997. Micropatterning fluid lipid bilayers on solid supports. *Science.* 275:651–653.
24. Salaita, K., P. M. Nair, …, J. T. Groves. 2010. Restriction of receptor movement alters cellular response: physical force sensing by EphA2. *Science.* 327:1380–1385.
25. Mossman, K. D., G. Campi, …, M. L. Dustin. 2005. Altered TCR signaling from geometrically repatterned immunological synapses. *Science.* 310:1191–1193.
26. Yu, C. H., J. B. Law, …, M. P. Sheetz. 2011. Early integrin binding to Arg-Gly-Asp peptide activates actin polymerization and contractile movement that stimulates outward translocation. *Proc. Natl. Acad. Sci. USA.* 108:20585–20590.
27. Caculitan, N. G., H. Kai, …, J. T. Groves. 2014. Size-based chromatography of signaling clusters in a living cell membrane. *Nano Lett.* 14:2293–2298.
28. Lohmüller, T., Q. Xu, and J. T. Groves. 2013. Nanoscale obstacle arrays frustrate transport of EphA2-Ephrin-A1 clusters in cancer cell lines. *Nano Lett.* 13:3059–3064.
29. DeMond, A. L., K. D. Mossman, …, J. T. Groves. 2008. T cell receptor microcluster transport through molecular mazes reveals mechanism of translocation. *Biophys. J.* 94:3286–3292.
30. Manz, B. N., B. L. Jackson, …, J. Groves. 2011. T-cell triggering thresholds are modulated by the number of antigen within individual T-cell receptor clusters. *Proc. Natl. Acad. Sci. USA.* 108:9089–9094.
31. Lin, W. C., C. H. Yu, …, J. T. Groves. 2010. Supported membrane formation, characterization, functionalization, and patterning for application in biological science and technology. *Curr. Protoc. Chem. Biol.* 2:235–269.
32. Nye, J. A., and J. T. Groves. 2008. Kinetic control of histidine-tagged protein surface density on supported lipid bilayers. *Langmuir.* 24:4145–4149.
33. Schindelin, J., I. Arganda-Carreras, …, A. Cardona. 2012. Fiji: an open-source platform for biological-image analysis. *Nat. Methods.* 9:676–682.
34. Thevenaz, P., U. E. Ruttimann, and M. Unser. 1998. A pyramid approach to subpixel registration based on intensity. *IEEE Trans. Image Process.* 7:27–41.
35. Azioune, A., N. Carpi, …, M. Piel. 2010. Protein micropatterns: a direct printing protocol using deep UVs. *Methods Cell Biol.* 97:133–146.
36. Groves, J. T., R. Parthasarathy, and M. B. Forstner. 2008. Fluorescence imaging of membrane dynamics. *Annu. Rev. Biomed. Eng.* 10:311–338.
37. Adams, C. L., Y. T. Chen, …, W. J. Nelson. 1998. Mechanisms of epithelial cell-cell adhesion and cell compaction revealed by high-resolution tracking of E-cadherin-green fluorescent protein. *J. Cell Biol.* 142:1105–1119.
38. Lambert, M., O. Thoumine, …, R. M. Mège. 2007. Nucleation and growth of cadherin adhesions. *Exp. Cell Res.* 313:4025–4040.
39. Fenz, S. F., R. Merkel, and K. Sengupta. 2009. Diffusion and intermembrane distance: case study of avidin and E-cadherin mediated adhesion. *Langmuir.* 25:1074–1085.

40. Shewan, A. M., M. Maddugoda, …, A. S. Yap. 2005. Myosin 2 is a key Rho kinase target necessary for the local concentration of E-cadherin at cell-cell contacts. *Mol. Biol. Cell.* 16:4531–4542.

41. Thomas, W. A., C. Boscher, …, S. Dufour. 2013. α-Catenin and vinculin cooperate to promote high E-cadherin-based adhesion strength. *J. Biol. Chem.* 288:4957–4969.

42. Dufour, S., R. M. Mège, and J. P. Thiery. 2013. α-catenin, vinculin, and F-actin in strengthening E-cadherin cell-cell adhesions and mechanosensing. *Cell Adhes. Migr.* 7:345–350.

43. Peng, X., L. E. Cuff, …, K. A. DeMali. 2010. Vinculin regulates cell-surface E-cadherin expression by binding to beta-catenin. *J. Cell Sci.* 123:567–577.

44. Yamada, S., and W. J. Nelson. 2007. Localized zones of Rho and Rac activities drive initiation and expansion of epithelial cell-cell adhesion. *J. Cell Biol.* 178:517–527.

45. Nguyen, T. N., A. Uemura, …, S. Yamada. 2010. Zyxin-mediated actin assembly is required for efficient wound closure. *J. Biol. Chem.* 285:35439–35445.

46. Sperry, R. B., N. H. Bishop, …, M. D. Hansen. 2010. Zyxin controls migration in epithelial-mesenchymal transition by mediating actin-membrane linkages at cell-cell junctions. *J. Cell. Physiol.* 222:612–624.

47. Noritake, J., T. Watanabe, …, K. Kaibuchi. 2005. IQGAP1: a key regulator of adhesion and migration. *J. Cell Sci.* 118:2085–2092.

48. Kourtidis, A., S. P. Ngok, …, P. Z. Anastasiadis. 2015. Distinct E-cadherin-based complexes regulate cell behaviour through miRNA processing or Src and p120 catenin activity. *Nat. Cell Biol.* 17:1145–1157.

49. Carisey, A., R. Tsang, …, C. Ballestrem. 2013. Vinculin regulates the recruitment and release of core focal adhesion proteins in a force-dependent manner. *Curr. Biol.* 23:271–281.

50. Groves, J. T. 2006. Spatial mutation of the T cell immunological synapse. *Curr. Opin. Chem. Biol.* 10:544–550.

51. Wu, S. K., and A. S. Yap. 2013. Patterns in space: coordinating adhesion and actomyosin contractility at E-cadherin junctions. *Cell Commun. Adhes.* 20:201–212.

52. Wu, Y., P. Kanchanawong, and R. Zaidel-Bar. 2015. Actin-delimited adhesion-independent clustering of E-cadherin forms the nanoscale building blocks of adherens junctions. *Dev. Cell.* 32:139–154.

53. Pruitt, B. L., A. R. Dunn, …, W. J. Nelson. 2014. Mechano-transduction: from molecules to tissues. *PLoS Biol.* 12:e1001996.

54. Henzler-Wildman, K., and D. Kern. 2007. Dynamic personalities of proteins. *Nature.* 450:964–972.

55. Biswas, K. H., and S. S. Visweswariah. 2011. Distinct allostery induced in the cyclic GMP-binding, cyclic GMP-specific phosphodiesterase (PDE5) by cyclic GMP, sildenafil, and metal ions. *J. Biol. Chem.* 286:8545–8554.

56. Biswas, K. H., S. Badireddy, …, S. S. Visweswariah. 2015. Cyclic nucleotide binding and structural changes in the isolated GAF domain of Anabaena adenylyl cyclase, CyaB2. *PeerJ.* 3:e882.

57. Escobar, D. J., R. Desai, …, C. J. Gottardi. 2015. α-Catenin phosphorylation promotes intercellular adhesion through a dual-kinase mechanism. *J. Cell Sci.* 128:1150–1165.

58. Solanas, G., C. Cortina, …, E. Batlle. 2011. Cleavage of E-cadherin by ADAM10 mediates epithelial cell sorting downstream of EphB signalling. *Nat. Cell Biol.* 13:1100–1107.

59. de Beco, S., C. Gueudry, …, S. Coscoy. 2009. Endocytosis is required for E-cadherin redistribution at mature adherens junctions. *Proc. Natl. Acad. Sci. USA.* 106:7010–7015.

60. Greene, A. C., S. J. Lord, …, J. T. Groves. 2014. Spatial organization of EphA2 at the cell-cell interface modulates trans-endocytosis of ephrinA1. *Biophys. J.* 106:2196–2205.

61. Smoligovets, A. A., A. W. Smith, and J. T. Groves. 2013. Ratiometric imaging of the T-cell actin cytoskeleton reveals the nature of receptor-induced cytoskeletal enrichment. *Biophys. J.* 105:L11–L13.

62. Smoligovets, A. A., A. W. Smith, …, J. T. Groves. 2012. Characterization of dynamic actin associations with T-cell receptor microclusters in primary T cells. *J. Cell Sci.* 125:735–742.

63. Yu, Y., N. C. Fay, …, J. T. Groves. 2012. Myosin IIA modulates T cell receptor transport and CasL phosphorylation during early immunological synapse formation. *PLoS One.* 7:e30704.

64. Yu, C. H., H. J. Wu, …, J. T. Groves. 2010. Altered actin centripetal retrograde flow in physically restricted immunological synapses. *PLoS One.* 5:e11878.

65. Yu, C. H., N. B. Rafiq, …, M. P. Sheetz. 2013. Integrin-matrix clusters form podosome-like adhesions in the absence of traction forces. *Cell Reports.* 5:1456–1468.

66. Mossman, K., and J. Groves. 2007. Micropatterned supported membranes as tools for quantitative studies of the immunological synapse. *Chem. Soc. Rev.* 36:46–54.

67. Harrison, O. J., X. Jin, …, B. Honig. 2011. The extracellular architecture of adherens junctions revealed by crystal structures of type I cadherins. *Structure.* 19:244–256.

68. Garg, S., S. C. Fischer, E. M. Schuman, and E. H. Stelzer. 2015. Lateral assembly of N-cadherin drives tissue integrity by stabilizing adherens junctions. *J. R. Soc. Interface.* 12:20141055.

69. Bunse, S., S. Garg, …, E. Schuman. 2013. Role of N-cadherin cis and trans interfaces in the dynamics of adherens junctions in living cells. *PLoS One.* 8:e81517.

Biophysical Journal, Volume *111*

Supplemental Information

Sustained α-catenin Activation at E-cadherin Junctions in the Absence of Mechanical Force

Kabir H. Biswas, Kevin L. Hartman, Ronen Zaidel-Bar, and Jay T. Groves

Biophysical Journal, Volume *111*

Supporting Material

Sustained *α*-catenin Activation at E-cadherin Junctions in the Absence of Mechanical Force

Kabir H. Biswas, Kevin L. Hartman, Ronen Zaidel-Bar, and Jay T. Groves

SUPPORTING MATERIAL

Sustained α-catenin activation at E-cadherin junctions in the absence of mechanical force

Kabir H. Biswas, Kevin L. Hartman, Ronen Zaidel-Bar, Jay T. Groves

SUPPORTING MATERIALS AND METHODS

Supported lipid bilayer preparation

Supported lipid bilayers were prepared as described previously (1). The lipids 1,2-dioleoyl-*sn*-glycero-3-phosphocholine (DOPC) or 1,2-dipalmitoyl-*sn*-glycero-3-phosphocholine (DPPC) were mixed in chloroform with 4 mole % of 1,2-dioleoyl-*sn*-glycero-3-[(N-(5-amino-1-carboxypentyl)iminodiacetic acid)succinyl] nickel salt (Ni-NTA-DOGS). These lipids were purchased from Avanti Polar Lipids (Alabaster, AL). To visualize bilayer coverage and fluidity, Marina Blue 1,2-dihexadecanoyl-*sn*-glycero-3-phosphoethanolamine (Marina Blue DHPE) purchased from Life Technologies (Carlsbad, CA) was added to some vesicle preparations at a concentration of 1 mol %.

In a round bottom flask, the chloroform was evaporated by rotary vacuum to leave a thin lipid film. The lipids were then resuspended in 2 mL of deionized water by either directly pipetting or incubating overnight at 4 °C followed by pipetting. The final lipid concentration was 0.5 mg/mL. The solution was kept chilled on ice and a probe-tip sonicator (Sonics Vibra Cell, Sonics & Material, Newton, CT) was used to generate small unilamellar vesicles (SUVs). Solid debris from the sonication process was removed by centrifuging the solution at 20,000 × g and 4 ºC for 4 h, and the supernatant containing the SUVs was transferred to a fresh tube. All lipid vesicles were stored at 4 ºC until further use.

Glass coverslips, used as supported bilayer substrates, were cleaned by sonication in a 1:1 mixture of isopropanol and water for 15 to 30 min. After extensive rinsing with water, coverslips were further cleaned by incubating either in fresh Piranha solution (3:1 mixture of H_2SO_4 : 30% H_2O_2) for 5 min or in 50% H_2SO_4 overnight followed by UV treatment in an enclosed UV Ozone generator (UV/Ozone ProCleaner Plus, Bioforce Nanosciences, Ames, IA) for 15-30 min. The glass coverslips were next washed thoroughly with water and dried under an N_2 stream. The self-assembly of lipid bilayers was performed by adding a 1:1 mixture of lipid vesicles and 2 × Tris-buffered saline (TBS; Sigma-Aldrich, St. Louis, MO) to the coverslips and incubating for 5 min. These bilayer-supporting coverslips were each assembled into Attofluor Cell Chambers (Life Technologies) for further experiments

Micropatterned supported lipid bilayer

Micron-scale patterned supported lipid bilayers were prepared on UV-patterned polymer coated glass substrates (2). Briefly, acid cleaned and UV treated glass cover slips were dried and incubated with Poly(L-lysine)-graft-poly(ethylene glycol)-Biotin (PLL-g-PEG) (PLL(20 kDa)-g-[3.4]-PEG(2 kDa)) PLL-PEG-biotin (Nanocs Inc, New York, USA) at a concentration of 1 mg/ml for 2 h, rinsed and dried under N_2 stream. Micropatterns were created on the substrates by deep UV etching of the PLL-PEG-biotin polymer coating using a photomask (Bonda Technology Pte Ltd, Singapore) containing transparent circular patterns of 2 μm diameter for 7.5 min. Substrates were then rinsed extensively with water to remove any leftover polymer and dried under N_2 stream. Bilayers were deposited on the nanopatterned substrates as described above.

Nanopatterned supported lipid bilayer

Glass coverslips patterned with chromium lines of 5 nm height, 100 nm width, and precisely defined pitches ranging from 0.5 – 2 μm were produced by nanoimprint lithography, as

described previously (3). First, a silicon-based imprint mold was patterned with nanoscale features by electron-beam lithography and etching. Piranha-cleaned glass coverslips were spin-coated with a layer of UV-curable polymer. Then, the imprint mold was pressed to transfer the pattern. The polymer coating was cured with UV light, and the residual polymer within the patterns was removed by oxygen plasma etching to expose the glass surface. Next, thermal evaporation was used to deposit a thin layer (~5 nm) of chromium over the entire region. Resist lift-off processing left the chromium deposited on the glass surface as the patterned lines, while removing the polymer and chromium elsewhere. Substrates were further cleaned as described in the previous section before depositing a lipid bilayer.

Functionalization of supported lipid bilayers with E-cad-ECD

E-cad-ECD was coupled to the supported membrane via the polyhistidine-Ni-NTA interaction. Although the kinetics of this interaction are known to be complex (4), it proves sufficiently stable for work with E-cad-ECD, partly due to the intrinsic stabilization achieved once the proteins assemble into clusters (5). Supported lipid bilayers assembled in Attofluor Cell Chambers were rinsed with 15 mL TBS and incubated with 0.008% BSA in TBS for 30 min to block non-specific binding. Bilayers were rinsed with a 15 mL solution of 1 mM $CaCl_2$ in TBS (TBS + Ca^{2+}). Human E-cad-ECD protein construct consisting of residues D155-I707, with a C-terminus polyhistidine tag (Sino Biologicals, Beijing, China) was diluted with TBS + Ca^{2+}, and added to the bilayer at a final concentration of 10 µg per sample in a total volume of ~1 ml. The samples were incubated at room temperature for 90 min, followed by rinsing with 15 mL TBS + Ca^{2+} to remove unbound protein from the solution. After another 30 min incubation, the bilayer was again rinsed with 15 mL imaging buffer (50 mM HEPES, 150 mM NaCl, 5 mM KCl, 1 mM $MgCl_2$, 11.1 mM D-glucose, 2 mM $CaCl_2$, pH 7.4) to both remove recently desorbed protein molecules from the solution (4) as well as to prepare the bilayers for live cell assays. For FRAP analysis, E-cad-ECD was

fluorescently labeled with Alexa Fluor647 (Life Technologies) using a protein labeling kit according to manufacturer's protocol.

Cell culture and preparation of cells for live cell experiments

MKN-28 cells stably expressing E-cad-GFP (6) were cultured at very low densities to maintain single cells in RPMI 1680 supplemented with 10% FBS and 1% penicillin-streptomycin, at 37 ºC and in an atmosphere of 5% CO_2. To prepare the cells for experiments, cells were washed with DPBS, and then detached from the surface by incubating with an enzyme-free dissociation buffer (Cell Stripper, Life Technologies), for 10 – 20 min at 37 ºC. The cells were pipetted gently to produce a single cell suspension, which was then centrifuged and resuspended in the imaging buffer (5). Cells were incubated for 10-15 min in the imaging buffer before seeding on the bilayers.

Assay for junction formation on bilayers

Single cell suspensions prepared as described above were seeded on either non-patterned or patterned bilayers pre-assembled into the Attofluor Cell Chambers and incubated at 37 ºC and in an atmosphere of 5% CO_2 for 1 h, and imaged by either total internal reflection fluorescence (TIRF) or confocal microscopy. For quantification of cell adhesion to bilayers, cells were seeded on bilayers prepared either without E-cad-ECD or with E-cad-ECD and incubated at 37 ºC and in an atmosphere of 5% CO_2 for 1 h. Post incubation, cells were washed with 15 mL of chilled Dulbecco's phosphate-buffered saline (DPBS) to remove unbound cells, and then fixed with 4% paraformaldehyde for 15 minutes at room temperature. Samples were imaged with a bright field microscope (10× objective) and cells were counted per frame. For experiments under reduced actomyosin tension, cells were seeded on bilayers and allowed to form junctions for 1 h and then subsequently treated with 50 μM Y-27632 for 30 min before fixation and permeabilization. While α-catenin is expected

to revert to the inactive, closed conformation rapidly upon Y-27632 treatment of the cells (7-10), we chose to investigate the conformational state of α-catenin after 30 min of Y-27632 treatment. This was done to allow cells to achieve a mechanically equilibrated, no/low force steady state.

Immuno-staining of fixed cells

After incubating the cells on the bilayer for 1 hour, samples were gently rinsed with chilled DPBS, and then fixed with 4% paraformaldehyde for 15 minutes at room temperature. To permeabilize cells, the samples were incubated with 0.1% Triton-X for 15 min at room temperature. Next, the samples were blocked with 0.04% BSA in DPBS for 30 min, and then immunostained with primary antibodies for 1 hour, at the manufacturer's recommended dilution. The antibody against the intercellular domain (ICD) of E-cadherin was purchased from BD Biosciences (Franklin Lakes, NJ). The antibodies against α-catenin and vinculin were purchased from (Sigma-Aldrich) and the α18 conformation specific antibody against the 'open' conformation of α-catenin was a kind gift from Prof. Akira Nagafuchi. The antibodies against IQGAP-1 and LPP were purchased from Santa Cruz Biotechnology (Dallas, TX) and the antibody against zyxin was purchased from Abcam (Cambridge, England). Next, the samples were incubated with fluorescent secondary antibodies (Life Technologies) for 30 min at the manufacturer's recommended dilution concentration. For staining actin, permeabilized cells were incubated with fluorescent phalloidin (Sigma-Aldrich) for 30 minutes. In the experiment where adhesion formation was assessed with Y-27632 pretreated cells (Figure S2A), F-actin was visualized by the expression of lifeact-mCherry in the cells.

Microscopy and image analysis

An Eclipse Ti inverted microscope (Nikon) with an Evolve EMCCD camera (Photometrics, Tucson, AZ) was used for epi-fluoresence, TIRF microscopy and RICM. TIRF microscopy

was performed using a 100× TIRF objective with a numerical aperture of 1.49 (Nikon) and an iChrome MLE-L - Multi Laser Engine as a laser source (Toptica Photonics, Munich, Germany). RICM was performed using a filter cube containing a 530/11 nm excitation filter and a 50/50 beam-splitter dichroic mirror. Some images, including those for 3D projections, were collected from an Eclipse Ti inverted microscope (Nikon) with a CSU-X1 confocal spinning disk unit (Yokogawa, Tokyo, Japan), and Evolve EMCCD camera (Photometrics). Images were collected in Metamorph (Molecular Devices, Sunnyvale, CA) and analyzed with either ImageJ (NIH, Bethesda, MD) or Fiji (11). FRAP experiments on bilayers were performed by partly closing the field diaphragm such that only a small field of view (15 – 30 μm) is illuminated. Lipid or protein fluorescence was photobleached by continuous excitation with high intensity light until about 20-40% fluorescence intensity was remaining. Following photobleaching, recovery of fluorescence in the photobleached area was recorded by imaging the bilayer for 2 min. Live cell FRAP experiment was performed by bleaching a small area (~2 μm diameter) of central assembly of E-cadherin clusters using high intensity laser and recovery was monitored by acquiring images every 15 s.

Colocalization of E-cadherin with F-actin, β-catenin and α-catenin at the peripheral and central clusters were performed using the Coloc2 plugin in Fiji. Adhesions were manually segregated into peripheral and central for the colocalization analysis. To determine the ratio of α18 and total α-catenin staining intensities, background intensities were subtracted and then images registered using the TurboReg plugin (12) in Fiji. Post alignment, total α-catenin image was used for automatic thresholding to select clusters and exclude background signal in the ratiometric analysis. Ratiometric images were then computed using the RatioPlus plugin (http://rsb.info.nih.gov/ij/plugins/ratio-plus.html) in Fiji (11).

In vitro pull-down experiment

The intracellular domain of E-cadherin was cloned into pGEX-6p1 vector for expression with a GST and His_{12} tag in bacterial cells (E-cad-ICD-His_{12}-GST). The protein was purified using Ni-NTA-His_{12} and used as such for the pull-down experiment. Monolayer culture of cells was lysed in a buffer containing 1×TBS, 0.1% TritonX-100, 1×Roche protease inhibitor cocktail. Purified E-cad-ICD was loaded on pre-equilibrated GSH beads and was interacted cell lysate prepared from MKN28-E-cad-GFP cells for 1 h at 4°C. Post-interaction, the beads were washed thrice with the lysis buffer and loaded on polyacrylamide gel for western blot detection of β-catenin, α-catenin and vinculin using specific antibodies described in the previous section.

SUPPORTING DATA

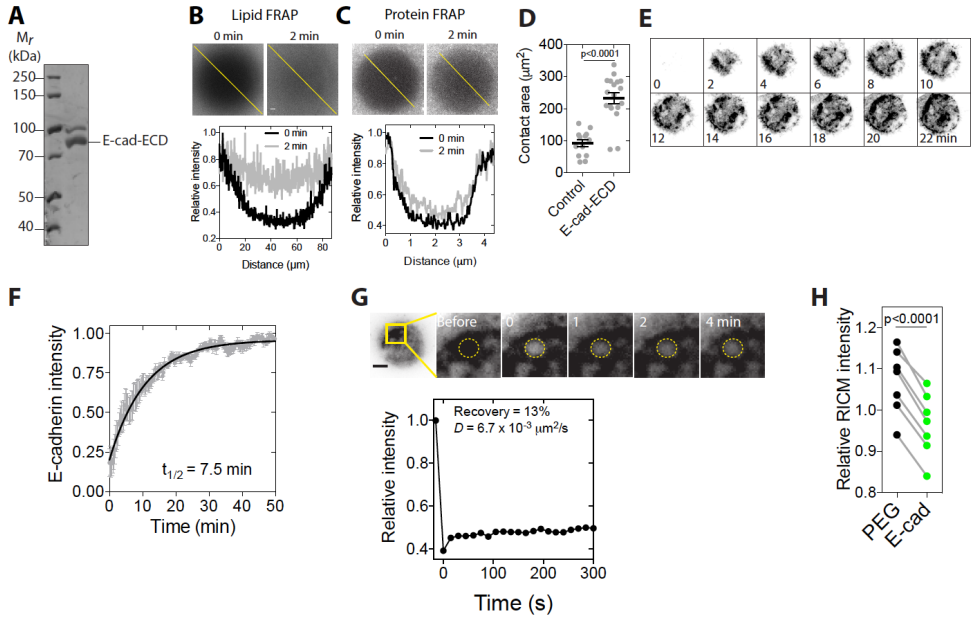

Figure S1 [A] SDS-PAGE analysis of the purified, recombinant mature human E-cad-ECD used for all reconstitution experiments. [B & C] FRAP analysis of Marina blue-DHPE lipid [B] and fluorescently labeled E-cad-ECD on supported lipid bilayer [C]. Plots below show relative intensity line scans performed on epi-fluorescence images acquired before and after 2 min of fluorescence recovery. Note that while the fluorescence intensity of the lipid molecules recover within 2 min, fluorescence intensity of E-cad-ECD does not, indicating a significantly reduced diffusion of E-cad-ECD on the bilayers. [D] A graph showing a greater contact area of cells adhering E-cad-ECD-functionalized bilayers in comparison to cells adhering to control bilayers without E-cad-ECD. Contact areas were determined from RICM images of many individual cells. p-value was obtained from unpaired t-test. [E] Time lapse TIRF microscopy images of cell forming adhesion on E-cad-ECD-functionalized bilayer showing E-cadherin cluster formation and their dynamic reorganization at the cell-bilayer interface. [F] A plot of relative E-cadherin-GFP intensity at the cell-bilayer interface determined from time-lapse TIRF microscopy images revealing the kinetics of E-cadherin

junction formation on supported lipid bilayer. Data shown is an average of multiple individual cells and was fit to a single exponential model to determine the half time ($t_{1/2}$ = 7.5 min) for junction maturation. [G] FRAP analysis of E-cadherin at an adhesion formed by a cell on an E-cad-ECD-functionalized bilayer performed by photobleaching E-cadherin-GFP in the cell. Dashed circles marks the photobleached area. Graph shows a small recovery of E-cadherin-GFP intensity over time, indicating immobilization of E-cadherin-GFP at the cell-bilayer contact. Scale bar, 5 μm. [H] Graph showing decrease in relative RICM intensity at sites of E-cadherin cluster formation compared to the rest of the non-specific cell bilayer contact from cells seeded on micropatterned bilayers containing bilayer discs of 2 μm in size. Data shown are paired RICM intensities obtained from multiple cells. p-value was obtained from a paired *t*-test.

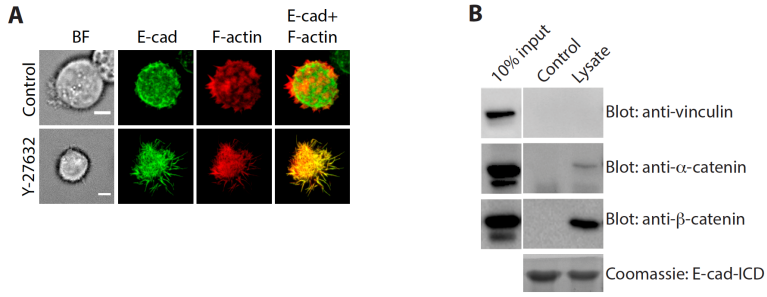

Figure S2 [A] Bright field (BF) and confocal images of E-cadherin and F-actin (Lifeact) in control and 50 μM Y-27632 pretreated cells revealing the requirement for actomyosin tension in the assembly of mature adhesions. [B] In vitro pull-down experiment with purified E-cadherin intracellular domain and lysates prepared from the MKN28-E-cad-GFP cells showing interaction of E-cadherin in solution with β-catenin and α-catenin, but not with vinculin. Scale bar, 5 μm.

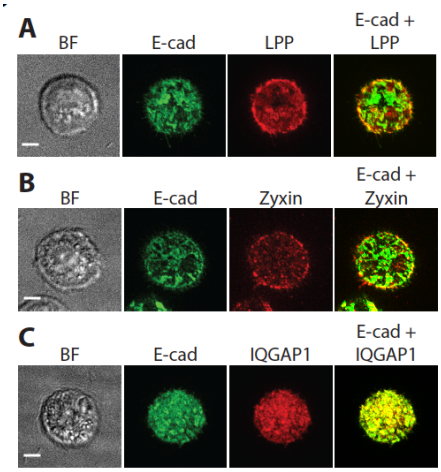

Figure S3 [A] to [C] BF and confocal images of E-cadherin-GFP expressing MKN28 cells forming junctions on E-cad-ECD-functionalized bilayers stained for LPP [A], Zyxin [B] and IQGAP1 [C]. While LPP and Zyxin co-localizes exclusively with peripheral assemblies of E-cadherin clusters, IQGAP1 co-localizes with both peripheral and central assemblies of E-cadherin clusters. Scale bar, 5 μm

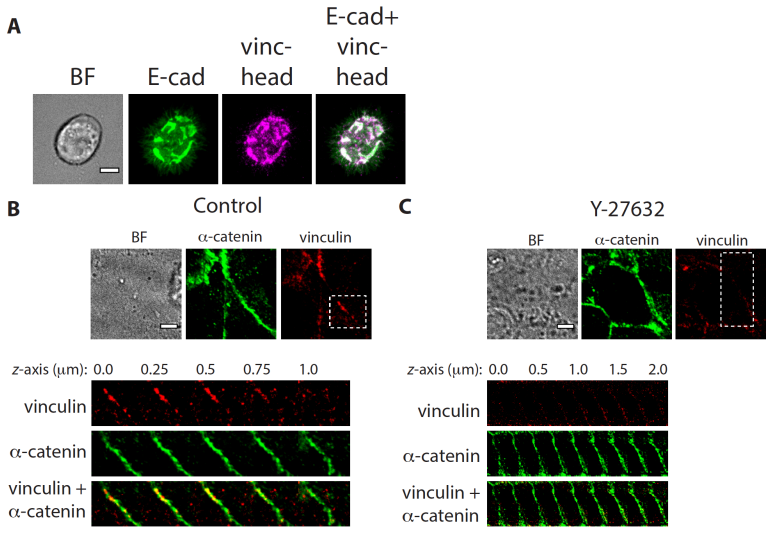

Figure S4. [A] BF and confocal images of vinculin-head-mCherry (vinc-head) expressing cells treated with 50 μM blebbistatin for 30 min after formation of adhesion on an E-cad-ECD bilayer. [B & C] BF and confocal images of cells without (control) [B] or with 30 min of 50 μM Y-27632 treatment [C] stained for α-catenin (total) and vinculin. Lower panels

show various confocal z-sections of the junction highlighted in the vinculin image. Note that apical staining for vinculin is lost in cells treated with 50 μM Y-27632. Scale bar, 5 μm

REFERENCES

1. Lin, W. C., C. H. Yu, S. Triffo, and J. T. Groves. 2010. Supported membrane formation, characterization, functionalization, and patterning for application in biological science and technology. Curr Protoc Chem Biol 2:235-269.
2. Azioune, A., N. Carpi, Q. Tseng, M. Thery, and M. Piel. 2010. Protein micropatterns: A direct printing protocol using deep UVs. Methods in cell biology 97:133-146.
3. Yu, C. H., J. B. Law, M. Suryana, H. Y. Low, and M. P. Sheetz. 2011. Early integrin binding to Arg-Gly-Asp peptide activates actin polymerization and contractile movement that stimulates outward translocation. Proceedings of the National Academy of Sciences of the United States of America 108:20585-20590.
4. Nye, J. A., and J. T. Groves. 2008. Kinetic control of histidine-tagged protein surface density on supported lipid bilayers. Langmuir : the ACS journal of surfaces and colloids 24:4145-4149.
5. Biswas, K. H., K. L. Hartman, C. H. Yu, O. J. Harrison, H. Song, A. W. Smith, W. Y. Huang, W. C. Lin, Z. Guo, A. Padmanabhan, S. M. Troyanovsky, M. L. Dustin, L. Shapiro, B. Honig, R. Zaidel-Bar, and J. T. Groves. 2015. E-cadherin junction formation involves an active kinetic nucleation process. Proceedings of the National Academy of Sciences of the United States of America 112:10932-10937.
6. Guo, Z., L. J. Neilson, H. Zhong, P. S. Murray, S. Zanivan, and R. Zaidel-Bar. 2014. E-cadherin interactome complexity and robustness resolved by quantitative proteomics. Science signaling 7:rs7.
7. Kim, T. J., S. Zheng, J. Sun, I. Muhamed, J. Wu, L. Lei, X. Kong, D. E. Leckband, and Y. Wang. 2015. Dynamic visualization of alpha-catenin reveals rapid, reversible conformation switching between tension states. Current biology : CB 25:218-224.
8. Yonemura, S., Y. Wada, T. Watanabe, A. Nagafuchi, and M. Shibata. 2010. alpha-Catenin as a tension transducer that induces adherens junction development. Nature cell biology 12:533-542.
9. Yao, M., W. Qiu, R. Liu, A. K. Efremov, P. Cong, R. Seddiki, M. Payre, C. T. Lim, B. Ladoux, R. M. Mege, and J. Yan. 2014. Force-dependent conformational switch of alpha-catenin controls vinculin binding. Nature communications 5:4525.
10. Buckley, C. D., J. Tan, K. L. Anderson, D. Hanein, N. Volkmann, W. I. Weis, W. J. Nelson, and A. R. Dunn. 2014. Cell adhesion. The minimal cadherin-catenin complex binds to actin filaments under force. Science 346:1254211.
11. Schindelin, J., I. Arganda-Carreras, E. Frise, V. Kaynig, M. Longair, T. Pietzsch, S. Preibisch, C. Rueden, S. Saalfeld, B. Schmid, J. Y. Tinevez, D. J. White, V. Hartenstein, K. Eliceiri, P. Tomancak, and A. Cardona. 2012. Fiji: an open-source platform for biological-image analysis. Nature methods 9:676-682.
12. Thevenaz, P., U. E. Ruttimann, and M. Unser. 1998. A pyramid approach to subpixel registration based on intensity. IEEE transactions on image processing : a publication of the IEEE Signal Processing Society 7:27-41.